Metal-Containing Zinc Phosphate EDI Zeolites Synthesized by Sol–gel Assisted Hydrothermal Method

Xuelei Wang [1,2,]*[ID], Zhaojun Dong [3,]*, Qiufeng Wang [4], Chao Meng [1], Weibin Zhuang [1], Jiyuan Liu [1], Ying Song [1], Yuxin Jin [1] and Shaobin Yang [1,2]

[1] College of Materials Science and Engineering, Liaoning Technical University, Fuxin 123000, China; mikko_mc@163.com (C.M.); wbzhuanglntu@163.com (W.Z.); s112965473@163.com (J.L.); songyingwork@163.com (Y.S.); jinyuxingo@126.com (Y.J.); lgdysb@163.com (S.Y.)
[2] Institute of Mineral Materials and Clean Transformation, Liaoning Technical University, Fuxin 123000, China
[3] College of New Energy and Environment, Jilin University, Changchun 130012, China
[4] School of Geomatics, Liaoning Technical University, Fuxin 123000 China; wangqioufeng@163.com
[*] Correspondence: wangxuelei-19@163.com (X.W.); dongzhaojun@jlu.edu.cn (Z.D.);
Tel.: +86-0418-511-0099 (X.W.); +86-0431-8516-8614 (Z.D.)

Abstract: Three different metal-containing zinc phosphate, $[C_3H_{12}N_2][Zn_{0.5}Fe_{1.5}(PO_4)_2]$ (1), $[C_3H_{12}N_2][Zn_{0.67}Co_{1.33}(PO_4)_2]$ (2) and $[C_3H_{12}N_2][Zn_{0.67}Ni_{1.33}(PO_4)_2]$ (3) with EDI topology were prepared by sol–gel assisted hydrothermal method. The advantages of this method are lower synthesis temperature and uniform mixing. The crystalline metal-containing zinc phosphate zeolites exhibit a variety of SEM morphologies because of the entanglement of three different metal ions. The zinc ions in the zinc phosphate EDI molecular sieve were partially substituted by Fe, Co and Ni ions. The ICP analysis shows that the metal ratios of Zn/M are 1/3, 1/2 and 1/2. Variable temperature susceptibility was measured on powder samples in the range 2–300 K. All three M-EDI molecular sieves exhibit antiferromagnetic properties. In addition, they were analyzed by XRD, CHN, IR and TG.

Keywords: EDI zeolite; zinc phosphate; sol–gel; hydrothermal; metal-containing; magnetic property

1. Introduction

Zeolites have been extensively studied due to their channel structure and potential applications in industrial catalysis, gas sorption, gas separations, oil cracking and so forth [1–5]. For example, SAPO-34 phosphate molecular sieve catalysts can provide an alternative platform for methanol conversion to olefins (MTO), which produces basic chemicals from nonparallel resources such as natural gas and coal [6]. This is due to substitution, which changes effectively the acidic active center of phosphate molecular sieve. Since the aluminophosphate zeolite was first reported in 1982 [7], many of aluminophosphate zeolite materials were found in related literatures [8–10]. As an example, AlPO-78 with a 24-layer ABC-6 aluminophosphate zeolite is one of the most recent study [11]. After more than two decades of development, a lot of researches on other metal phosphate zeolite materials have been done for replacing or mixing aluminophosphate [12–14]. Some novel zeolite structures can be easily formed due to the difference in metal atom radius and coordination ability, such as metal mixing aluminophosphate MAPO-CJ40 containing one-dimensional (1D) helical 10-ring channels [15], monoatomic substituted gallophosphate zeolite involving a 20-ring extra-large channels [16] and diatomic substituted cobalt-gallium phosphate zeolite with two-dimensional (2D) 12-ring and 10-ring interconnected channel along the [1 0 0] and [0 −1 1] directions [17]. It can be found that the account of main group metal phosphate zeolites is major in the reported literatures [18–20].

In recent years, researchers have paid more attention to the performances of zinc phosphate zeolite materials [21]. Zeolites are also found in nature, they originally exist as minerals, but their important commercial values have led to extensive academic and industrial research on their syntheses, structures and various properties. Zinc phosphate molecular sieves have been replaced and mixed to break their limitations, so that they can play a unique role in magnetism, electricity, optics, etc. [22]. Advance to the present, zinc phosphate molecular sieves contain multiple topologies [23]. Among them, zinc phosphate ($[C_6H_{14}N_2][Zn_2(PO_4)_2]$) with the edingtonite framework topology structure is reported by our research group [24]. In order to extend the performance and application of these zinc phosphate molecular sieves, many studies have been done on metal substitution of zinc phosphate zeolites [25–30]. In addition, suitable synthetic methods are also helpful for studying the properties of zinc phosphate molecular sieve materials [31]. In the past decades, conventionally hydrothermal and solvothermal synthesis methods are often used to synthesize zinc phosphate molecular sieves [32]. However, some new methods are less tried [33]. Sol–gel synthetic method [34], which is a multipurpose synthesis process through transitioning the status from a "sol" into a "gel" in the preparation of materials, is currently gaining widespread attention [35]. With the aim of researching zinc phosphate molecular sieves with interesting magnetic properties, we prepared three open-framework metal-substituted zinc phosphate zeolites $[C_3H_{12}N_2][Zn_{0.5}Fe_{1.5}(PO_4)_2]$ (1), $[C_3H_{12}N_2][Zn_{0.67}Co_{1.33}(PO_4)_2]$ (2) and $[C_3H_{12}N_2][Zn_{0.67}Ni_{1.33}(PO_4)_2]$ (3) with EDI topology by sol–gel assisted hydrothermal method [36]. Combining the advantages of hydrothermal and sol–gel method, the reaction temperature was lower than that of other phosphates, the product was uniformly mixed without impurities. Interestingly, they contain antiferromagnetic properties.

2. Materials and Methods

2.1. Materials

Reagents were purchased and not further purified. These mainly contained phosphorous acid (H_3PO_3, 99%, Aladdin Chemistry Co., Ltd., Shanghai, China), zinc acetate dihydrate ($Zn(OAc)_2 \cdot 2H_2O$, 99%, Sinopharm Chemical Reagent Co., Ltd., Shanghai, China), iron trichloride hexahydrate ($FeCl_3 \cdot 6H_2O$, 99%, Sinopharm Chemical Reagent Co., Ltd., Shanghai, China), cobaltous acetate tetrahydrate ($Co(OAc)_2 \cdot 4H_2O$, 99%, Sinopharm Chemical Reagent Co., Ltd., Shanghai, China), nickel chloride hexahydrate ($NiCl_2 \cdot 6H_2O$, 98%, Sinopharm Chemical Reagent Co., Ltd., Shanghai, China), 1,3-propanediamine ($C_3H_{10}N_2$, 99%, 0.86 g/mL, Aladdin Chemistry Co., Ltd., Shanghai, China), isobutanol ($C_4H_{10}O$, 99%, 0.81 g/mL, Liaoning Quan Rui Reagent Co., Ltd., Shenyang, China) and demonized water (18.2 MΩ·cm, N50-DI Deionizer, Dongguanshi Naibaichuan Water Treatment Equipment Co., Ltd., Dongguan, China).

2.2. Synthesis

To synthesize metal-containing zinc phosphate molecular sieve $[C_3H_{12}N_2][Zn_{0.5}Fe_{1.5}(PO_4)_2]$ (1), as shown in Figure 1, the 1,3-propanediamine organic base dissolves in water to get solution A. The zinc acetate and iron trichloride were dissolved in isobutanol and phosphorous acid was added to obtain solution B. Under the condition of stirring for 1 h, solution A was added to solution B slowly through syringe. After that, we can discover that solution B had changed to a sol state. After 3 h of aging, the sol turned into a gel. The gel was put into the 50 mL reactor as fast as possible and heated for 72 h at 160 °C to obtain the target product (1) molecular sieve. Compared with conventional hydrothermal synthesis [24], products prepared by sol–gel assisted hydrothermal synthesis have perfect shape and were prepared at lower heat treatment temperature. The final products were rinsed twice with demineralized water and dried in the air. $[C_3H_{12}N_2][Zn_{0.67}Co_{1.33}(PO_4)_2]$ (2) and $[C_3H_{12}N_2][Zn_{0.67}Ni_{1.33}(PO_4)_2]$ (3) molecular sieves were prepared from same process, in which $Zn(OAc)_2 \cdot 2H_2O$, metal salt, 1,3-propanediamine, H_3PO_3, isobutanol and demineralized water were mixed with the optimum mole ratio of 1.0:1.0:10.0:5.0:100:1000.
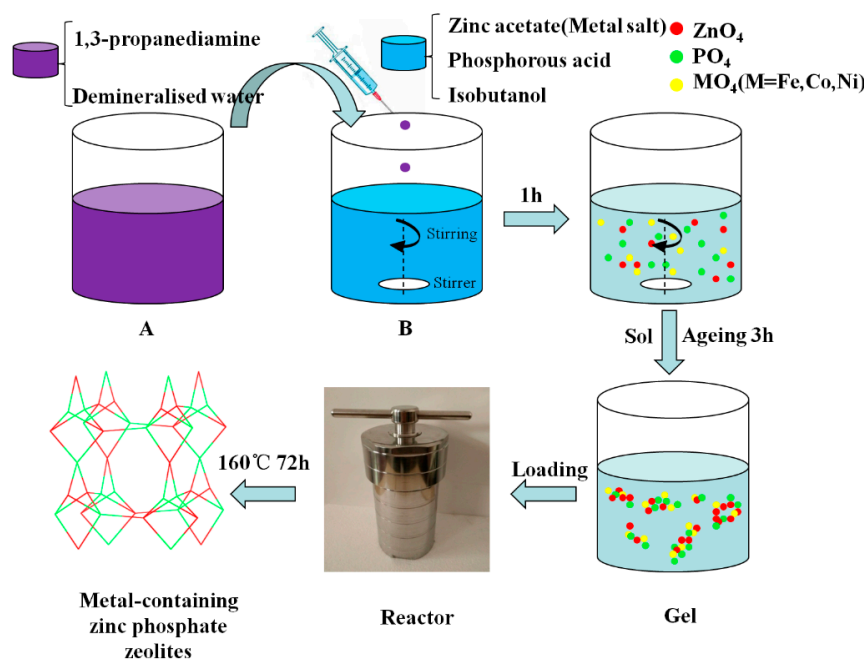
Figure 1. Schematic route to synthesize metal-containing zinc phosphate zeolites.

2.3. Characterization

The surface morphology of samples was characterized by using JEOL JSM-7500F (JEOL, Tokyo, Japan) scanning electron microscopy (SEM) device. The powder X-ray diffraction (XRD) data were measured by using Rigaku 2500 X-ray diffractometer (Cu Kα radiation, λ = 1.5418 Å) device (Rigaku, Tokyo, Japan). Zn, Fe, Co, Ni and P elements were analyzed by using the Perkin-Elmer Optima 3300 DV inductive coupled plasma (ICP) spectrometer (Perkin-Elmer, Waltham, MA, USA). Determination of C, N and H elements were conducted on a Perkin-Elmer 2400 elemental (CHN) analyzer (Perkin-Elmer, Waltham, MA, USA). Thermal gravimetric (TG) analyses of samples were performed on a device of Netzsch Sta 449F3 (Netzsch, Selb, Germany)with a heating rate of 30 °C/min. Infrared spectrum (IR) data were detected on Nicolet Impact 410 FTIR spectrometer (Nicolet, New York, NY, USA) in a wavenumber range of 4000–400 cm^{-1}. Magnetic properties were performed using MPMS SQUID XL magnetometer (Quantum Design, San Diego, CA, USA) in the range of 2–300 K temperature under an applied field of 1 kOe external magnetic field.

3. Results and Discussion

3.1. Synthesis and Characterization

Different-colored metal-containing zinc phosphate products were synthesized by sol–gel assisted hydrothermal method. The metal-containing zinc phosphate molecular sieves had wide synthetic conditions, and could be synthesized within this range Zn salt, metal salt, organic amine, H$_3$PO$_3$, organic solvent and H$_2$O with the mole ratio of 1.0:1.0:6.0–10.0:4.0–8.0:60–100:500–1000. Zinc salt could be zinc acetate or zinc chloride organic amine could be 1,2-propanediamine or trielenediamine and the organic solvent was isobutanol or isopropanol. The photographs of the metal-containing zinc phosphate zeolites synthesized under optimal conditions are shown in Figure 2. The color of molecular sieve (1) is dark green, the color of molecular sieve (2) is dark blue, and the color of molecular sieve (3) is light green. When metal-containing zinc phosphate zeolites were prepared according to the different ratio, the morphologies of the products by SEM observation were different. The morphology of molecular sieve (1) was an imperfectly crystallized block under minimum amount of organic solvents and water conditions (Figure 3a), and the perfectly crystallized oblong block-shaped crystals were synthesized using the optimum mole ratio (Figure 3b). Similarly, zeolite (2) had square

block morphology (Figure 3c,e), while molecular (3) sieve was a truncated cube block morphology (Figure 3d,f). When the amount of organic solvent and water was less, the morphologies of crystals appeared twin and transgranular phenomenon occurred. This is because more organic pure solvents and water reagents will help crystals to grow better [37]. The morphologies of the three metals replacing phosphate molecular sieves are different because of the different amount of metal substitution. In addition, such presence of different ions makes the preferred orientation of crystals changing.
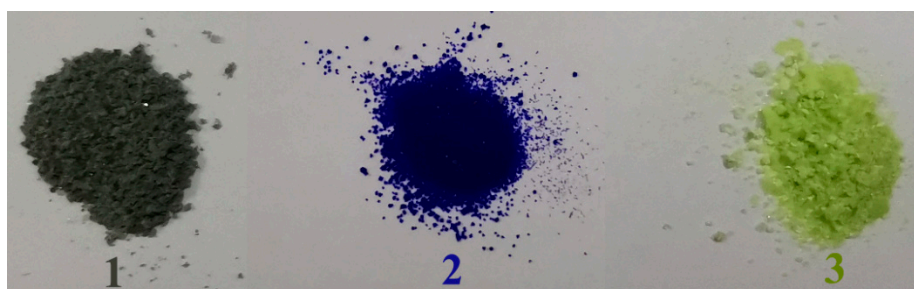

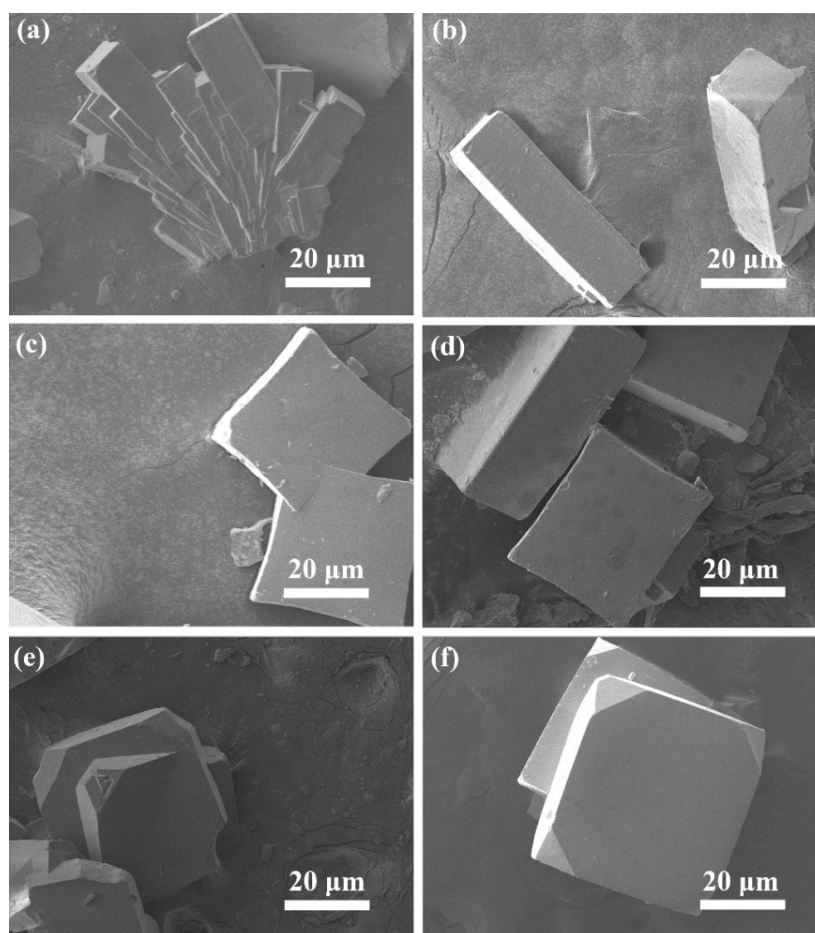**Figure 2.** Photographs of the three metal-containing zinc phosphate products.

Figure 3. SEM images of (**a**) (1) synthesized by minimum amount of organic solvents and water, (**b**) (1) synthesized by the optimum mole ratio, (**c**) (2) synthesized minimum with amount of organic solvents and water, (**d**) (2) synthesized using the optimum mole ratio, (**e**) (3) synthesized minimum amount of organic solvents and water and (**f**) (3) synthesized using the optimum mole ratio.

Additionally, the simulated and experimental XRD data of three metal-containing zinc phosphate molecular sieves were tested. It can be found that the XRD data obtained from three experiments of

metal-containing zinc phosphate have a good agreement with the simulation of $[C_6H_{14}N_2][Zn_2(PO_4)_2]$ EDI zeolite (Figure 4) [24]. The crystal data are as follows: Tetragonal crystal system, *P*-42$_1$*c* space group, *a* = *b* = 9.9611(8) Å, *c* = 12.800(2) Å, *α* = *β* = *γ* = 90.00°. A little bit different is that the position of the main peak of the feature moved in a small angular position. This is caused by the different radii of the substituted metal ions. For metal cations of the same period, the larger the atomic number, the smaller the radius and the larger the pore are, the position of diffraction peak will be slightly shifted to a small angle [38]. Compared with Fe, Co, Ni and Zn ions, their radius decreases step by step, and the pore size of the molecular sieve increases, so the diffraction peak of XRD slightly changes to the smaller 2theta position. The ICP and CHN data of three metal-containing zinc phosphate zeolites are shown in Table 1. From the ratio of metal atomic content, it can be concluded that Zn/Fe is about 1/3, Zn/Co is about 1/2, and Zn/Ni is about 1/2. The ratio relationship between each atom conforms to the zinc phosphate EDI zeolite [39].
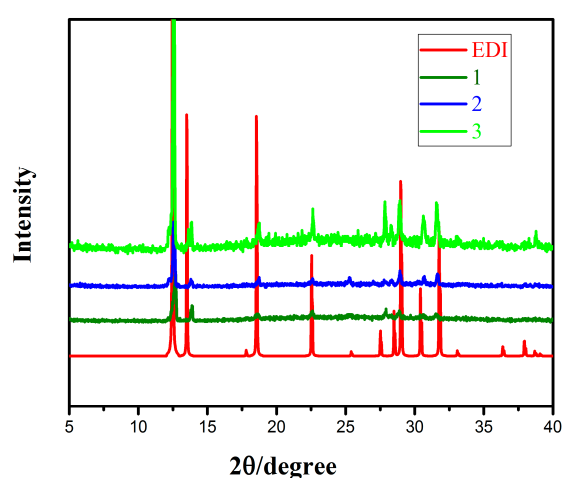

Figure 4. Simulated XRD pattern of EDI and experimental XRD patterns of three metal-containing zinc phosphate zeolite.

Table 1. The ICP and CHN data of the three metal-containing zinc phosphate zeolites studied in the present work (wt. %).

Element	(1)	Range	SD	(2)	Range	SD	(3)	Range	SD
Zn	8.03	7.98–8.07	0.03	10.78	10.72–10.81	0.04	10.82	10.75–10.85	0.03
M	23.76	23.52–23.86	0.05	20.12	20.01–20.28	0.05	20.89	20.73–20.97	0.04
P	15.94	15.78–16,03	0.06	15.89	15.78–15.95	0.03	15.90	15.76–16.03	0.06
C	9.36	9.25–9.43	0.04	9.21	9.10–9.32	0.04	9.25	9.16–9.33	0.03
H	3.28	3.24–3.30	0.02	3.09	3.01–3.13	0.02	3.11	3.03–3.18	0.02
N	7.38	7.31–7.42	0.03	7.18	7.02–7.32	0.04	7.20	7.08–7.26	0.03

The TG curve of three metal-containing zinc phosphate zeolites show in Figure 5. TG for zeolite (1) exhibits a weight loss of 20.01%, which is attributed to the 1,3-propanediamine organic amine molecules (calc. 20.02%). For zeolite (2), the observed decrease of 19.36% between 450 and 800 °C corresponded well to the organic amine molecules (calc. 19.48%). The TG curve of zeolite (3) shows a weight decrease of 19.51% (calc. 19.56%). In addition, the weight loss interval is different for three metal-containing zinc phosphate zeolites. The zeolite (2) can be stabilized to 450 °C, while zeolites (1) and (3) only stabilize to 300 °C. For IR analysis, the organic amine molecules and PO$_4$ -functional groups were mainly analyzed. Therefore, the molecular sieve (2) is chosen as the representative to analyze. The IR spectrum (Figure 6) exhibits typical changes for zeolite (2). The interrupted bands at 1070, 786, 680, 570 and 470 cm^{-1} are owing to the vibration of P-O bonds [40]. Absorption peaks at 1606, 3335 and 3550 cm^{-1} are due to the bending and stretching vibrations of N-H bonds. The absorption peaks at 3245 cm^{-1} and 3165 cm^{-1} are related to the stretching vibration of C-H bonds.
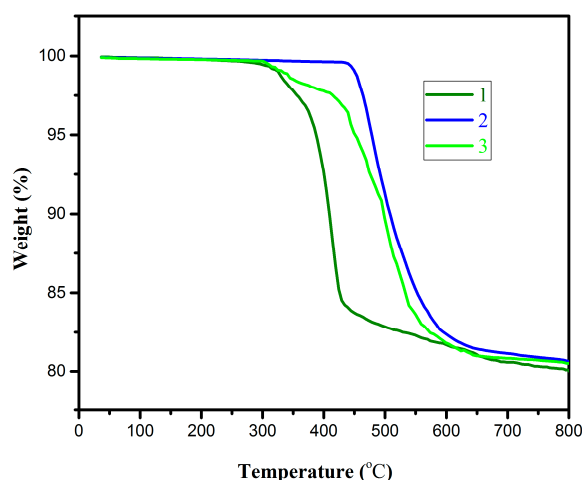
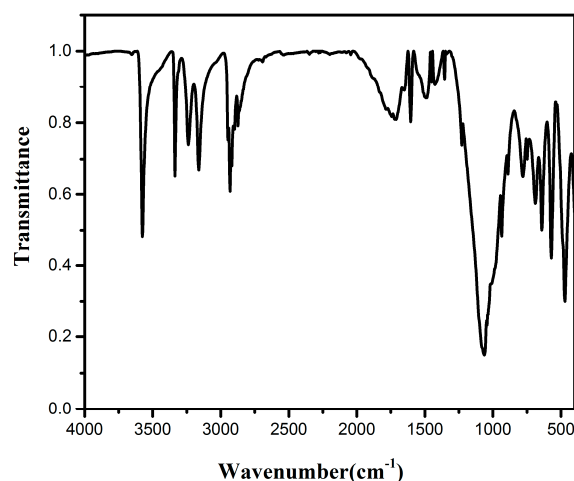**Figure 5.** TG curves of the three metal-containing zinc phosphate EDI zeolites studied in the present work.

Figure 6. IR spectra of zeolite (**2**).

3.2. Magnetic Properties

For the three metal-containing zinc phosphate zeolites studied in this work, variable temperature susceptibility (χ) of powder samples was measured in the range 2–300 K. As shown in Figure 7a, the molar magnetic susceptibility (χ_m) of zeolite (1) increased with decrease of temperature above 3 K and had an inflection point at 3 K. This phenomenon indicated that it had a long-range magnetic ordering, which proved to be an antiferromagnetic interaction between Fe ions in zeolite (1) [41]. In the range of 30–300 K, The plot of $1/\chi_m$ vs. T obeys the Curie-Weiss law with Curie constant Weiss constant θ = −29.93 K and C_m = 3.95 cm^3·K·mol^{-1}, and the formula is listed as follows:

$$\chi = C/(T - \theta) \tag{1}$$

This negative θ value further confirmed the antiferromagnetic interactions within zeolite (1). For the zeolite (2), it also showed similar behavior (Figure 7b). The χ_m decreased with increasing temperature decrease in the high temperature of 50–300 K and zeolite (2) gave values of θ = −33.13 K and C_m = 3.11 cm^3·K·mol^{-1}. The negative value of θ and peak appearing at about 3 K suggested that the interaction between the Co ions was antiferromagnetic. Unlike zeolites (1) and (2) the χ_m vs. T plot of zeolite (3) exhibited a single change throughout the cooling process, the χ_m decreased with increasing temperature decrease (Figure 7c). The high temperature data were also fitted the

Curie–Weiss equation. It exhibited the values of $\theta = -19.02$ K and $C_m = 2.05$ cm^3·K·mol^{-1} in the range 50–300 K. The negative θ values further indicated that the antiferromagnetic interactions existed in zeolite (3). By comparing the magnetic curves of three metal-containing zinc phosphate zeolites, zeolites (1) and (2) were different from 3 in the low temperature region. However, the overall change of χ_m vs. T plots and their negative θ values indicated existence of antiferromagnetic interactions.
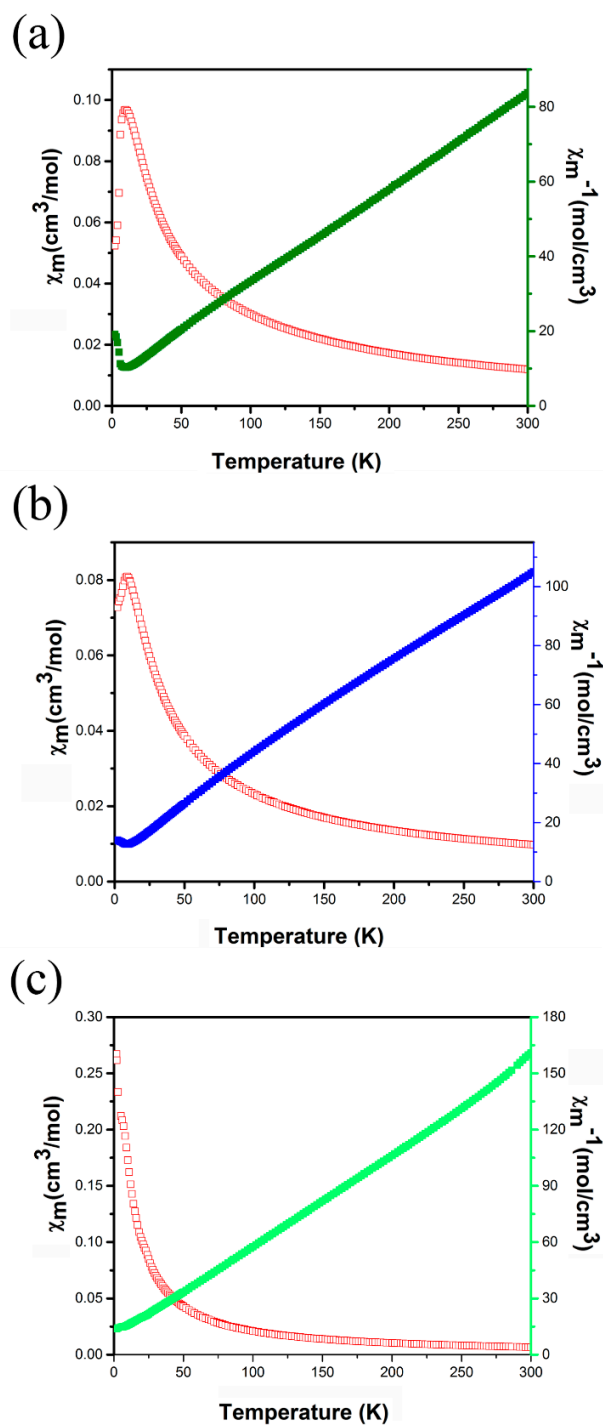

Figure 7. (**a**) Thermal evolution of χm and χm^{-1} curves for (**a**) zeolite (1), (**b**) zeolite (2) and (**c**) zeolite (3). For χm curves, each zeolite is represented in red; For χm^{-1} curves, zeolite (1) is represented in dark green, zeolite (2) is represented in blue and zeolite (3) is represented in light green.

4. Conclusions

Three open-framework metal-substituted zinc phosphate EDI zeolites were prepared by sol–gel assisted hydrothermal method. The products prepared by this method have perfect shape and were prepared at a lower heat treatment temperature. They get the oblong block-shaped, square block and truncated cube block morphology, respectively. At the same reaction condition, the metal ratios of the three metal-containing zinc phosphate molecular sieves are 1/3, 1/2 and 1/2. The three kinds of metal-containing zinc phosphate molecular sieves have strong antiferromagnetic properties. In terms of application, metal-containing zinc phosphate EDI zeolites change effectively the acidic active center of molecular sieve, so it can be applied to acid catalysis. In addition, the introduction of magnetism makes the molecular sieve have anti-ferromagnetic characteristics, which has research value for the application of molecular sieve in magnetic research. The successful synthesis of three metal-containing zinc phosphate zeolites is helpful for studying the substitution of metal for zeolites and exploring more microporous materials with novel structures and properties. The next step is to study the influence of metal substitution on the change of acid center molecular sieve, the catalytic properties of molecular sieves will be studied.

References

1. Cheetham, A.K.; Férey, G.; Loiseau, T. Open-framework inorganic materials. *Angew. Chem. Int. Ed.* **1999**, *38*, 3268–3292. [CrossRef]
2. Davis, M.E. Ordered porous materials for emerging applications. *Nature* **2002**, *417*, 813–821. [CrossRef] [PubMed]
3. Murugavel, R.; Choudhury, A.; Walawalkar, M.G.; Pothiraja, R.; Rao, C.N.R. Metal complexes of organophosphate esters and open-framework metal phosphates: Synthesis, structure, transformations, and applications. *Chem. Rev.* **2008**, *108*, 3549–3655. [CrossRef] [PubMed]
4. Li, J.; Corma, A.; Yu, J. Synthesis of new zeolite structures. *Chem. Soc. Rev.* **2015**, *44*, 7112–7127. [CrossRef] [PubMed]
5. Kragović, M.; Daković, A.; Marković, M.; Krstić, J.; Gatta, G.D.; Rotiroti, N. Characterization of lead sorption by the natural and Fe(III)-modified zeolite. *Appl. Surf. Sci.* **2013**, *283*, 764–774. [CrossRef]
6. Yang, M.; Fan, D.; Wei, Y.; Tian, P.; Liu, Z. Recent Progress in Methanol-to-Olefins (MTO) Catalysts. *Adv. Mater.* **2019**, *31*, 1902181. [CrossRef]
7. Wilson, S.T.; Lok, B.M.; Messina, C.A.; Cannan, T.R.; Flanigen, E.M. Aluminophosphate molecular sieves: A new class of microporous crystalline inorganic solids. *J. Am. Chem. Soc.* **1982**, *104*, 1146–1147. [CrossRef]
8. MeurigáThomas, J. Synthesis and characterization of a novel extra large ring of aluminophosphate JDF-20. *J. Chem. Soc. Chem. Commun.* **1992**, *12*, 875–876.
9. Wei, Y.; Tian, Z.; Gies, H.; Xu, R.; Ma, H.; Pei, R.; Zhang, W.; Xu, Y.; Wang, L.; Li, K. Ionothermal synthesis of an aluminophosphate molecular sieve with 20-ring pore openings. *Angew. Chem. Int. Ed.* **2010**, *49*, 5367–5370. [CrossRef]
10. Seo, Y.; Lee, S.; Jo, C.; Ryoo, R. Microporous aluminophosphate nanosheets and their nanomorphic zeolite analogues tailored by hierarchical structure-directing amines. *J. Am. Chem. Soc.* **2013**, *135*, 8806–8809. [CrossRef]
11. Yuhas, B.D.; Mowat, J.P.; Miller, M.A.; Sinkler, W. AlPO-78: A 24-layer ABC-6 aluminophosphate synthesized using a simple structure-directing agent. *Chem. Mater.* **2018**, *30*, 582–586. [CrossRef]

12. Zhang, H.; Chen, M.; Shi, Z.; Bu, X.; Zhou, Y.; Xu, X.; Zhao, D. Hydrothermal synthesis of new pure beryllophosphate molecular sieve phases from concentrated amines. *Chem. Mater.* **2001**, *13*, 2042–2048. [CrossRef]

13. Nenoff, T.M.; Harrison, W.T.; Gier, T.E.; Stucky, G.D. Room-temperature synthesis and characterization of new ZnPO and ZnAsO sodalite open frameworks. *J. Am. Chem. Soc.* **1991**, *113*, 378–379. [CrossRef]

14. Yuan, H.-M.; Chen, J.-S.; Zhu, G.-S.; Li, J.-Y.; Yu, J.-H.; Yang, G.-D.; Xu, R.-R. The first organo-templated cobalt phosphate with a zeolite topology. *Inorg. Chem.* **2000**, *39*, 1476–1479. [CrossRef]

15. Song, X.; Li, Y.; Gan, L.; Wang, Z.; Yu, J.; Xu, R. Heteroatom-stabilized chiral framework of aluminophosphate molecular sieves. *Angew. Chem. Int. Ed.* **2009**, *48*, 314–317. [CrossRef]

16. Estermann, M.; McCusker, L.; Baerlocher, C.; Merrouche, A.; Kessler, H. A Synthetic gallophosphate molecular sieve with a 20-tetrahedral-atom pore opening. *Nature* **1991**, *352*, 320–323. [CrossRef]

17. Josien, L.; Simon-Masseron, A.; Gramlich, V.; Patarin, J.; Rouleau, L. Synthesis and crystal structure of IM-6, a new open framework cobalt–gallium phosphate with ten- and twelve-membered pore openings. *Chemistry* **2003**, *9*, 856–861. [CrossRef]

18. Seo, S.; Yang, T.; Shin, J.; Jo, D.; Zou, X.; Hong, S. Two aluminophosphate molecular sieves built from Pairs of enantiomeric structural building units. *Angew. Chem. Int. Ed.* **2018**, *130*, 3789–3794. [CrossRef]

19. Wang, B.; Mu, Y.; Zhang, H.; Shi, H.; Chen, G.; Yu, Y.; Yang, Z.; Li, J.; Yu, J. Red room-temperature phosphorescence of CDs@zeolite composites triggered by heteroatoms in zeolite frameworks. *ACS Cent. Sci.* **2019**, *5*, 349–356. [CrossRef]

20. Wang, Y.; Li, Y.; Yan, Y.; Xu, J.; Guan, B.; Wang, Q.; Li, J.; Yu, J. ChemInform abstract: Luminescent carbon dots in a new magnesium aluminophosphate zeolite. *Chem. Commun.* **2013**, *49*, 9006–9008. [CrossRef]

21. Wu, J.; Yan, Y.; Liu, B.; Wang, X.; Li, J.; Yu, J. Multifunctional open-framework zinc phosphate| $C_{12}H_{14}N_2$|[$Zn_6(PO_4)_4(HPO_4)(H_2O)_2$]: Photochromic, photoelectric and fluorescent properties. *Chem. Commun.* **2013**, *49*, 4995–4997. [CrossRef] [PubMed]

22. Tao, C.; Wu, J.; Yan, Y.; Shi, C.; Li, J. A new methylviologen-templated zinc gallophosphate zeolite with photo-/thermochromism, fluorescent and photoelectric properties. *Inorg. Chem. Front.* **2016**, *3*, 541–546. [CrossRef]

23. Gier, T.; Stucky, G. ChemInform abstract: Low-temperature synthesis of hydrated zinco(beryllo)phosphate and arsenate molecular sieves. *Nature* **1991**, *349*, 508–510. [CrossRef]

24. Wang, X.; Zhou, Y.; Dong, Z.; Meng, C.; Li, X.; Hong, X.; Yang, S. The effects of different dimensional organic amines on synthetic zinc phosphites/phosphates. *J. Porous. Mater.* **2020**, *27*, 21–28. [CrossRef]

25. Ke, Y.; He, G.; Li, J.; Zhang, Y.; Lu, S. A new mixed divalent metal phosphate with zeolite thomsonite framework topology. *New J. Chem.* **2001**, *25*, 1627–1630.

26. Helliwell, M.; Helliwell, J.; Kaucic, V.; Zabukovec Logar, N.; Barba, L.; Busetto, E.; Lausi, A. Determination of the site of incorporation of cobalt in CoZnPO-CZP by multiple-wavelength anomalous-dispersion crystallography. *Acta Crystallogr. Sec. B Struct. Sci.* **1999**, *55*, 327–332. [CrossRef]

27. Ng, H.Y.; Harrison, W.T.A. Monoclinic NaZnPO4-ABW, a new modification of the zeolite ABW structure type containing elliptical eight-ring channels. *Microporous Mesoporous Mater.* **1998**, *23*, 197–202. [CrossRef]

28. Chippindale, A.; Cowley, A.; Peacock, K. Synthesis and characterisation of [TH][$ZnGaP_2O_8$] (T = CN_3H_5 and C_4NH_9); Two microporous zinc-gallium phosphates with the gismondine structure. *Microporous Mesoporous Mater.* **1998**, *24*, 133–141. [CrossRef]

29. Bu, X.; Gier, T.; Feng, P.; Stucky, G. Template control of framework topology and charge in new phosphate- and arsenate-based sodalite analogs. *Microporous Mesoporous Mater.* **1998**, *20*, 371–379. [CrossRef]

30. Tusar, N.N.; Kaucic, V.; Geremia, S.; Vlaic, G. A zinc-rich CHA-type aluminophosphate. *Zeolites* **1995**, *15*, 708–713. [CrossRef]

31. Ng, E.P.; Ghoy, J.P.; Awala, H.; Vicente, A.; Adnan, R.; Ling, T.C.; Mintova, S. Ionothermal synthesis of FeAPO-5 in the presence of phosphorous acid. *Crystengcomm* **2016**, *18*, 257–265. [CrossRef]

32. Shao, L.; Li, Y.; Yu, J.; Xu, R. Divalent-Metal-Stabilized Aluminophosphates Exhibiting a New Zeolite Framework Topology. *Inorg. Chem.* **2012**, *51*, 225–229. [CrossRef] [PubMed]

33. Dell'Era, A.; Pasquali, M.; Bauer, E.; Vecchio, S.; Scaramuzzo, F.; Lupi, C. Synthesis, Characterization, and Electrochemical Behavior of LiMnxFe(1 − x)PO4 Composites Obtained from Phenylphosphonate-Based Organic-Inorganic Hybrids. *Materials* **2017**, *11*, 56. [CrossRef] [PubMed]

34. Catauro, M.; Tranquillo, E.; Dell'Era, A.; Tuffi, R.; Vecchio, S. Thermal behavior and structural study of ZrO$_2$/poly(ε-caprolactone) hybrids synthesized via sol–gel route. *Ceram. Int.* **2018**, *45*, 2771–2778. [CrossRef]

35. Catauro, M.; Tranquillo, E.; Barrino, F.; Blanco, I.; Dal Poggetto, F.; Naviglio, D. Drug release of hybrid materials containing Fe(II) citrate synthesized by sol–gel technique. *Materials* **2018**, *11*, 2270. [CrossRef]

36. Chen, D.; Huang, F.; Bing, C.; Caruso, R. Mesoporous Anatase TiO$_2$ Beads With High Surface Areas and Controllable Pore Sizes: A Superior Candidate for High-Performance Dye-Sensitized Solar Cells. *Adv. Mater.* **2009**, *21*, 2206–2210. [CrossRef]

37. Feng, G.; Cheng, P.; Yan, W.; Boronat, M.; Li, X.; Su, J.-H.; Wang, J.; Li, Y.; Corma, A.; Xu, R.; et al. Accelerated crystallization of zeolites via hydroxyl free radicals. *Science* **2016**, *351*, 1188–1191. [CrossRef]

38. Wang, X.; Zhang, J.; Yang, S.; Yan, H.; Hong, X.; Dong, W.; Liu, Y.; Zhang, B.; Wen, Z. Interlayer space regulating of NiMn layered double hydroxides for supercapacitors by controlling hydrothermal reaction time. *Electrochim. Acta* **2019**, *295*, 1–6. [CrossRef]

39. Harrison, W. [H$_3$N(CH$_2$)$_3$NH$_3$]$_{0.5}$[ZnPO$_4$], an organically templated zincophosphate analogue of the aluminosilicate zeolite edingtonite. *Acta Crystallogr. E Struct. Pep. Online* **2001**, *57*, 248–250. [CrossRef]

40. Wang, K.C.; Li, T.; Zeng, H.M.; Zou, G.H.; Zhang, Q.H.; Lin, Z.E. Ionothermal synthesis of open-framework metal phosphates using a multifunctional ionic liquid. *Inorg. Chem.* **2018**, *57*, 8726–8729. [CrossRef]

41. Lin, Z.E.; Nayek, H.P.; Dehnen, S. Flux synthesis of three-dimensional open-framework zinc phosphite and manganese phosphite-oxalate with 12-ring channels. *Microporous Mesoporous Mater.* **2009**, *126*, 95–100. [CrossRef]